Interphase formation with carboxylic acids as slurry additives for Si electrodes in Li-ion batteries. Part 1: performance and gas evolution

IOP Publishing J. Phys. Energy 5 (2023) 025003 https://doi.org/10.1088/2515-7655/acbbed

Journal of Physics: Energy

OPEN ACCESS

RECEIVED
14 October 2022

REVISED
20 January 2023

ACCEPTED FOR PUBLICATION
14 February 2023

PUBLISHED
3 March 2023

PAPER

Interphase formation with carboxylic acids as slurry additives for Si electrodes in Li-ion batteries. Part 1: performance and gas evolution

Fabian Jeschull[1,*], Leiting Zhang[2], Łukasz Kondracki, Flora Scott and Sigita Trabesinger[*]

Battery Electrodes and Cells, Electrochemistry Laboratory, Paul Scherrer Institute, Forschungsstrasse 111, Villigen PSI, 5232, Switzerland
[1] Current affiliation: Institute for Applied Materials - Energy Storage Systems (IAM-ESS), Karlsruhe Institute of Technology (KIT), Hermann-von-Helmholtz-Platz 1, 76 344 Eggenstein-Leopoldshafen, Germany.
[2] Current affiliation: Department of Chemistry – Ångström Laboratory, Uppsala University, 75 121 Uppsala, Sweden.
[*] Authors to whom any correspondence should be addressed.

E-mail: fabian.jeschull@kit.edu and sigita.trabesinger@psi.ch

Keywords: lithium-ion battery, Si, citric acid, electrode slurry, OEMS

Supplementary material for this article is available online

Abstract

Rendering the solid electrolyte interphase and the inter-particle connections more resilient to volume changes of the active material is a key challenge for silicon electrodes. The slurry preparation in a buffered aqueous solution offers a strategy to increase the cycle life and capacity retention of silicon electrodes considerably. So far, studies have mostly been focused on a citrate buffer at $pH = 3$, and therefore, in this study a series of carboxylic acids is examined as potential buffers for slurry preparation in order to assess which chemical and physical properties of carboxylic acids are decisive for maximizing the capacity retention for Si as active material. In addition, the cycling stability of buffer-containing electrodes was tested in dependence of the buffer content. The results were complemented by analysis of the gas evolution using online electrochemical mass spectrometry in order to understand the SEI layer formation in presence of carboxylic acids and effect of high proton concentration.

1. Introduction

Silicon has long been considered the 'holy grail' for lithium-ion battery (LIB) applications, owing to its high theoretical gravimetric capacity (3579 mAh g^{-1} for $Li_{15}Si_4$) in comparison to conventional graphite negative electrodes (372 mAh g^{-1}) [1]. However, the tremendous volume expansion during the alloying reaction with lithium results in rapid capacity fading as a result of electronic contact loss and repeated stress-induced cracking of the solid electrolyte interphase (SEI) [2–5]. In order to maintain the interparticle contacts in Si electrodes, binders, such as carboxymethylcellulose sodium salt (CMC-Na) or polyacrylic acid (PAA), have been suggested as alternatives to the established poly (vinylidene difluoride) (PVdF)-based polymers [6–11]. It has been as well reported that the capacity retention of CMC-Na-containing electrodes can be further improved if a citrate buffer at $pH = 3$ is used during slurry preparation, incidentally, PAA generates aqueous slurries of a similar pH [12–14].

The origins of resulting improvements are manifold. Early studies suggested that a silyl ester-bond, Si-O-C(=O)-R, between the Si surface and the electrode binder is formed [7, 12, 13]. Atomic force microscopy experiments supported the conclusion that a covalent bond is formed between the Si particles and the binder, rendering the composite more resilient to volume changes [15]. Lucht and co-workers found that the presence of citric acid alone (using PVdF binder) can improve the capacity retention of the Si electrode [16, 17], arguing that citric acid forms a silyl ester on the silicon surface itself, as confirmed by Fourier-transform infrared spectroscopy - attenuated total reflection (FTIR-ATR) measurements. Recently, citric acid has also been applied as a slurry additive (in aqueous slurries) for the preparation of positive electrodes, e.g. lithium manganese nickel oxides [18, 19]. In agreement with previous studies, the authors

found that citric acid undergoes a crosslinking reaction with the CMC-Na binder [20, 21]. Such crosslinking reaction would render the binder more rigid and form a composite network more resilient towards Si particle expansion [22]. Lestriez and coworkers further improved the electrode properties in a 3 d maturation step at high humidity, which, in presence of carboxylic acids, reinforces both the particle network and the adhesion to the copper current collector [23–26]. Lastly, Wei and Obrovac [27] and Nguyen *et al* [28] reported that carboxylic acids as flocculation suppressants also improve the particle dispersion.

The different interpretations on the binder-buffer-surface interactions are obviously related and all three mechanism might contribute to the final electrode coating properties. Our group has recently revisited previous FTIR results and mechanistic interpretations [29], where a comprehensive and comparable set of FTIR spectra was provided for three different carboxylic acids in different Si-electrode-relevant environments. The results proved that various carboxylic acids interact strongly with the Si surface itself. Electrodes prepared in a malate buffer, for example, showed similar improvements in capacity retention to those prepared in a citrate buffer. However, the number of studies that have looked at alternative carboxylic acids [27, 29] or, in the broader scope, oligomeric additives (e.g. poly(acrylic-co-maleic)acid, PAMA) [4, 28] is so far very narrow. In general, it would be desirable to replace citric acid by a lighter carboxylic acid, in order to decrease the dead weight in the final electrode formulation [29].

The significant performance improvements by simply replacing water by a low-*pH* buffer in the slurry preparation process is appealing as a straightforward, viable and effective strategy. However, the role of the carboxylic acid during the slurry preparation and at the electrode-electrolyte interaction level is not well understood and deeper knowledge by using specialized analytical tools needs to be acquired.

Parameters that could have an impact on the electrochemical behavior, when carboxylate buffer are employed, include the acid strength, i.e. its pK_a-value, which determines the ratio between carboxylic groups (COOH) and its conjugate base (COO^-) (COO^-/COOH ratio) at any given *pH* (in this study $pH = 3$). High concentrations of acidic protons could potentially trigger electrolyte degradation reactions [30] and affect the SEI formation process adversely. Other parameters may include the density of functional groups, the chain length of the compound's backbone and its polarity (all of which are to a certain degree reflected in the pK_a-value as well).

Therefore, in this study, we aim to address three basic questions regarding the electrode preparation process with carboxylic acids and their influence on the SEI formation:

(1) What are the prerequisites of carboxylic acids in terms of their inherent properties (e.g. pK_a-value) and structural features that lead to performance improvements in Si electrodes?
(2) How the buffer amount affects the performance and is there an optimal value?
(3) Does the buffer affect the SEI formation process in its early stages?

Firstly, we examine a range of different carboxyl acids that are structurally derived from the citric acid molecule to establish structural carboxylic-acid features leading to improved performance, answering the first question. Then the focus is on citric-acid-buffered Si electrodes with different buffer contents, answering the second question. Finally, for the first time, online electrochemical mass spectrometry (OEMS) results are presented on this type of electrodes with the aim to understand how the presence of high-proton concentrations in a slurry affect the SEI formation during the first cycles, using citric acid as a model buffer, and answering the third and final question of this study.

2. Experimental

2.1. Materials

Silicon nanoparticles (30–50 nm, >98%) were purchased from Nanostructured & Amorphous Materials Inc. (Houston, USA). The conductive additive SuperC45 was provided by Imerys Graphite & Carbon. CMC-Na (Alfa Aesar, Lot No.: 102 14813, degree of substitution: 0.82, viscosity 522 mPa s (1% @ 25 °C)) and lithium foil (750 μm, >99.9%, Alfa Aesar) was obtained from Alfa Aesar. Glassfiber separators (EUJ 116, Hollingsworth & Vose, UK) were dried prior use at 150 °C overnight under vacuum. Copper foil (20 μm) was supplied by Schlenk Metallfolien, Germany. The electrolyte comprising of 96 wt.% LP30 (1 M $LiPF_6$ in EC:DMC, v/v = 1:1, BASF) and 4 wt.% fluoroethylene carbonate (FEC, BASF) was used. Formic acid, glycolic acid (>99%), acetic acid (>99%), hexanoic acid (caproic acid, >99%), DL-tartaric acid (>99%), DL-malic acid (99%), succinic acid (>99%), adipic acid (>99%), citric acid (>99.5%), and sodium citrate tribasic dehydrate (>99.5%) were purchased from Sigma-Aldrich and used as received. Butane-1,2,3,4-tetracarboxylic acid (>98%) was purchased from Chemie Brunschwig AG.

Table 1. Electrode formulations prepared in various buffered aqueous solutions. An A^- refers to the amount of NaOH that was added to generate the buffer solution (except for AcAc and CitAc buffers).

Sample	Buffer	n(HA)/ 100 ml[b] (mmol)	n(A^-)/ 100 ml[b] (mmol)	Slurry *pH*	Buffer conc. (mm)	Solid content[a] (wt.%)	Si content (wt.%)
Si-CitAc-0 mm	No buffer		—	7	0	16.4	80
Si-CitAc-52 mm	Citric acid	4.26	0.93	3	52	14.8	75.6
Si-CitAc-100 mm	Citric acid	8.20	1.80	3	100	15.0	72.1
Si-CitAc-200 mm	Citric acid	16.42	3.60	3	200	14.8	65.4
Si-CitAc-294 mm	Citric acid	23.94	5.43	3	294	14.5	59.6
Si-ForAc	Formic acid	10	3.08	3	100	15.6	78.7
Si-GlyAc	Glycolic acid	10	1.59	3	100	15.9	77.1
Si-AcAc	Acetic acid	8.49	1.51	3	100	15.2	77.7
Si-TartAc	Tartaric acid	10	4.92	3	100	15.3	74.5
Si-MalAc	Malic acid	10	2.48	3	100	16.5	75.2
Si-SucAc	Succinic acid	10	1.01	3	100	14.5	74.9
Si-HexAc	Hexanoic acid	9.04	0.06	3	90	15.2	75.4
Si-AdiAc	Adipic acid	10	0.40	3	100	16.4	75.2
Si-BuTert-100 mm	1,2,3,4-butanetetra-carboxylic acid	10	3.45	3	100	15.4	71.3

Electrode compositions

Sample	Si content (wt.%)	CB content (wt.%)	Binder content (wt.%)	Carboxylic acid content (wt.%)	AM loading (electrode loading) (mg cm^{-2})
Si-CitAc-0 mm	80	12	8	0	1.60 (2.00)
Si-CitAc-52 mm	75.6	11.3	7.7	5.3	1.45 (1.87)
Si-CitAc-100 mm	72.1	10.8	7.1	10	1.52 (2.10)
Si-CitAc-200 mm	65.4	9.7	6.4	18.4	1.38 (2.09)
Si-CitAc-294 mm	59.6	8.7	6	25.6	2.88 (4.32)
Si-ForAc	78.7				2.05 (2.61)
Si-GlyAc	77.1	11.4	7.7	3.7	1.71 (2.22)
Si-AcAc	77.7	11.4	7.7	3.1	1.69 (2.11)
Si-TartAc	74.5	10.9	7.1	7.4	1.55 (2.10)
Si-MalAc	75.2	11.2	7.5	6.1	1.66 (2.21)
Si-SucAc	74.9	11.2	7.7	6.3	1.64 (2.19)
Si-HexAc	75.4	11.4	7.4	5.8	1.61 (2.13)
Si-AdiAc	75.2	10.8	7.3	6.6	1.71 (2.27)
Si-BuTert-100 mm	71.3	10.9	7.3	5.7	1.54 (2.15)

[a] including Si, carbon black, CMC-Na and the buffer.
[b] A^- refers to NaOH amount added to a 100 mm carboxylic acid stock solution during titration to $pH = 3$; exception: AcAc & CitAc (acid and conjugate acid were used instead).

2.2. Buffer preparation

The buffer preparation follows the procedure described in our previous work [29]. The acetate and citrate buffers were prepared by dissolving their sodium salts and the conjugate carboxylic acids in deionized water in a base-to-acid ratio of 1.51 mmol/8.49 mmol and 1.8 mmol/8.2 mmol (trisodium citrate/citric acid), respectively, yielding a 100 mm buffer solution at *pH* 3.

The remaining buffer mixtures were prepared by titration of a 100 mm aqueous solution of the respective carboxylic acids with 100 mm NaOH. The *pH* of the resulting solutions was controlled with a *pH* meter (Mettler Toledo Secen Multi with an InLab 413 *pH* sensor). The ratios between NaOH and acid are given in table 1.

2.3. Electrode preparation

The electrodes contained Si, SuperC45 and CMC-Na in a mass ratio of 8:1.2:0.8. As slurry medium deionized water or the buffered carboxylic-acid solutions described above, have been used. A detailed description of the electrode preparation is provided in [29]. A summary of the prepared electrode formulations and their precise active material contents is given in table 1.

Electrodes for the OEMS study were prepared in a similar way, coating the as-prepared slurry on a Cu-mesh (3CU6-0321FSR, max hole size of 0.254 mm, Dexmet Cooperation, USA) by doctor blade

technique with a wet thickness of 100 μm. After being punched into round discs of 18 mm in diameter, the electrodes were further dried under vacuum overnight at 120 °C, before being introduced to an Ar-filled glovebox.

2.4. Cell assembly and galvanostatic cycling

The dried electrodes were tested in lithium half-cells using a coin-cell-type setup [31]. Lithium was punched in 13 mm- diameter discs. The electrodes were spaced by 3 glassfiber separators, which were soaked by 500 μl of electrolyte (LP30 + 4 wt.% FEC). The cells were closed with a torque wrench in order to provide a constant and reproducible stack pressure.

The cells were conditioned during the first cycle with a C/25 (1 C = 3579 mAh g^{-1}) constant current-constant potential (CC-CP) charge and discharge cycle (potential cut-off (CC-step): 5 mV and 1.5 V, current cut-off (CV-step): C/50). In subsequent cycles, the charging current was increased to C/10 (potential cut-off (CC-step): 5 mV, current cut-off (CV-step): C/20). The discharging current was increased to C/3 (potential cut-off (CC-step): 1.5 V, current cut-off (CV-step): C/20). As shown in table 1, the active material content of the electrodes depends on the type of carboxylic acid used and the concentration of the buffer, and Si content varied between 70 and 80%. As a common basis for comparison, the current densities for any formulation were referred to the unbuffered (0 mm) Si electrode. This means that all electrodes experienced a current density (C-rate) corresponding to an unbuffered Si electrode with 80 wt.% active material content. With respect to buffered electrodes, this alters the C-rate of these electrodes slightly, as the real active material content was smaller. However, larger deviations (>5%) in current density are only observed for buffer concentrations >100 mm (citric acid series) and the Si-BuTert-100 mm sample (due to higher molecular mass of Butane-1,2,3,4-tetracarboxylic acid). The reason for this particular choice of the current density will be elaborated in the results and discussion section.

2.5. OEMS

The OEMS setup was described elsewhere [32] and operates with a quadrupole mass spectrometer (QMS 200, Pfeiffer) for partial pressure measurements, a pressure transducer (PAA-33X, Keller Druck AG) for total cell pressure, temperature, and internal volume determination, stainless steel gas pipes and Swagelok fittings (3 mm compression tube fittings, Swagelok, OH, USA) to connect the OEMS cells, and a set of solenoid valves (2-way magnetic valve, Series 99, silver-plated nickel seal, Parker) and a scroll pump (nXDS15i, EDWARDS GmbH) for efficient flushing. The magnetic valves are electronically controlled with a Solid State Relay Module (NI 9485 measurement system, National Instruments) connected to a computer with LabView software (NI Labview 2013, National Instruments). Calibration was carried out for ion-current signals from the mass spectrometer for signals at $m/z = 2$ (H_2), 26 (C_2H_4) and 44 (CO_2) using calibration gas bottles (1000 ppm of the respective gas in Ar).

In an in-house OEMS cell, lithium discs with 20 mm in diameter were used as the counter and reference electrodes, one piece of Celgard 2400 as separator, and 240 μl of LP30-FEC-mixed electrolyte. The cells were equilibrated at open circuit potential for 4 h prior to cyclic voltammetry (CV) measurement between 0.005 and 1.5 V vs. Li^+/Li at 30 μV s^{-1} scan rate for two cycles. To evaluate the gas evolution during slurry preparation, 10 mg of pristine nano-Si powders was directly placed in the OEMS cell, while 200 μl of either 100 mm of citrate buffer solution or deionized water (reference) were injected by a syringe. Gaseous products were analyzed using the LabView software.

3. Results and discussion

3.1. Impact of buffer type on capacity retention

The carboxylic acids in used in the first part of this study are divided in four groups (scheme 1): (1) monocarboxylic acids (formic (ForAc-1), acetic (AcAc-1), glycolic (GlyAc-1) & hexanoic acid (HexAc-1)), (2) bicarboxylic acids (succinic (SucAc-2), malic (MalAc-2), adipic (AdiAc-2) and tartaric acid (TarAc-2)), (3) tricarboxylic acid (citric acid, CitAc-3) and (4) tetracarboxylic acid (Butane-1,2,3,4-tetracarboxylic acid, ButAc-4).

The number behind the acids' abbreviation indicates its number of carboxyl-groups in the molecule. We have included monocarboxylic acids to assess the role of crosslinking reactions between carboxylic acid and binder. AcAc-1 for example would be able to undergo esterification reactions without forming crosslinks in the process, while GlyAc-1 still has the possibility to interact through it is additional -OH functionality. An overview of the carboxylic acid and buffer properties is given in table 2.

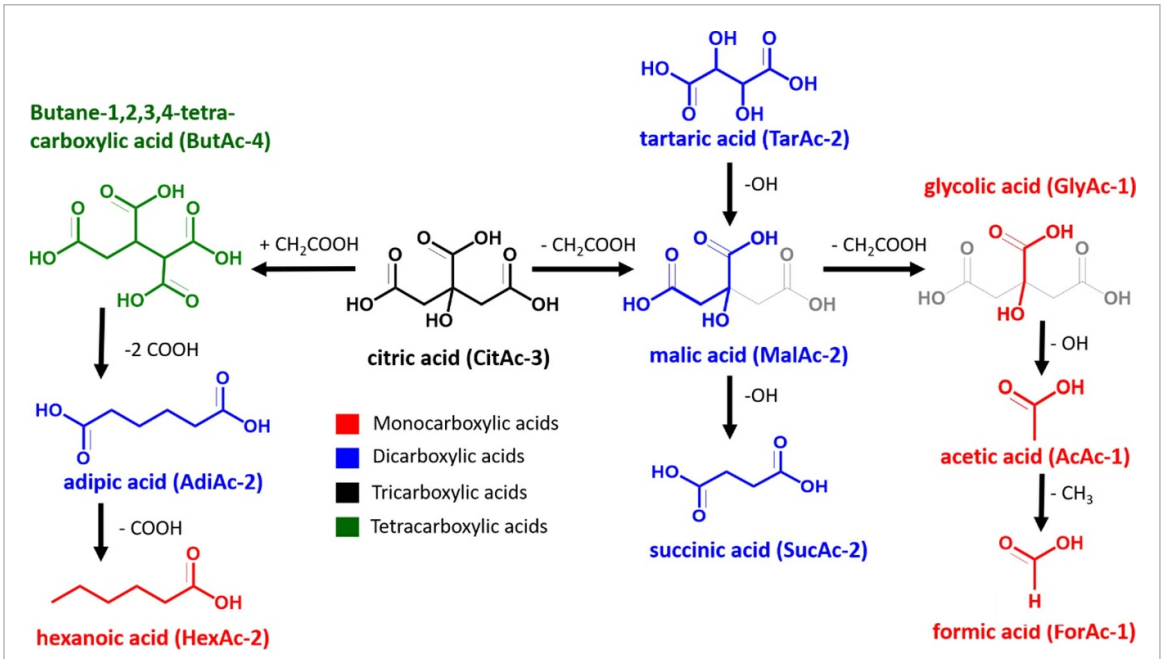

Scheme 1. Structural representation of carboxylic acids.

Table 2. Properties of carboxylic acids and corresponding buffers (100 mm, *pH* 3).

Carboxylic acid	Abbrev.	n(COOH)	M(acid)/ g mol^{-1}	pKa [33]	(COO^-)/ (COOH) ratio	m.p. °C[a]	b.p. C[a]
Formic acid	ForAc-1	1	46.0	3.75	0.30	8	101
Glycolic acid	GlyAc-1	1	76.1	3.83	0.16	75	—
Acetic acid	AcAc-1	1	60.1	4.76	0.017	16	118
Hexanoic acid	HexAc-1	1	116.2	4.9	0.007	−4	203
Tartaric acid	TarAc-2	2	150.1	3.03/4.37	0.25	210	—
Malic acid	MalAc-2	2	134.1	3.40/5.11	0.12	131	—
Succinic acid	SucAc-2	2	118.1	4.21/5.64	0.05	184	235
Adipic acid	AdiAc-2	2	146.1	4.41/5.41	0.02	151	265[c]
Citric acid	CitAc-3	3	192.1	3.13/4.76/6.40	0.18	153	—
Butane-1,2,3,4-tetracarboxylic acid	ButAc-4	4	234.1	3.4/4.4/5.5/6.6	0.09	195	—

[a] according to supplier information ('—', if no data available).
[b] [A^-] and [HA] refer to the equivalent concentration of carboxylic groups (normality/normal conc).
c@100 mmHg.

3.1.1. Capacity retention in Si‖Li half cells

The carboxylic acids presented in Scheme 1 have related structures. The carboxyl and hydroxyl groups are gradually removed from the reference molecule of the citric acid, figuratively speaking, (or added in the case of ButAc-4) so as to investigate their impact on the cell performance. The carboxylic acids were partly deprotonated to yield buffer solutions with $pH = 3$ at a buffer concentration of 100 mm. The thus-prepared buffers were then used for the preparation of Si electrode slurries.

Because the capacity fading of Si electrodes is mass-loading dependent [34–36], the Si loading was controlled in a close range of 1.4–1.7 mg_{Si} cm^{-2} (exception Si-ForAc). The capacity retention during galvanostatic cycling of the different electrode formulations is shown in figure 1. The discharge capacities and corresponding Coulombic efficiencies (C.E.) for the individual experiments are provided in figures S1(a)–(k). In general, the cycling data show that most Si electrodes treated in a buffer solution during slurry preparation exhibit better capacity retention, compared to a buffer-free Si electrode prepared in deionized water ($pH = 7$). Differences between cycling performance of electrodes with the same formulation may arise from the aforementioned mass loading discrepancies. Also, the electrode coatings were not optimized towards adhesion and cohesion strength, which resulted in brittle coatings that were delicate to handle. Poor adhesion properties on the copper substrate could lead readily to coating disconnection and are related,

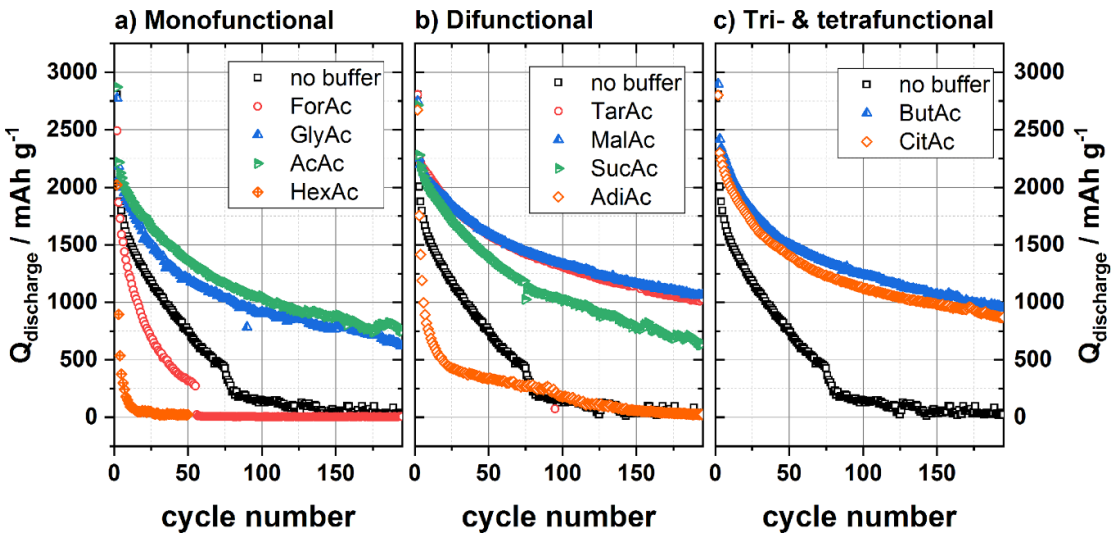

Figure 1. Galvanostatic cycling of Si electrodes prepared in buffers from (a) monofunctional, (b) difunctional and (c) tri- & tetrafunctional carboxylic acids.

amongst other parameters, to binder depletion at the current-collector/coating interface during drying [37, 38].

The cycling data can be summarized as follows: except the three carboxylic acids (ForAc-1, HexAc-2 and AdiAc-2), all other carboxylic-acid-containing electrodes show better capacity retentions than the Si electrode prepared in deionized water at neutral *pH*. The best capacity retention, with about 1000 mAh g^{-1} remaining after 200 cycles, are achieved by samples treated with di-, tri- or tetracarboxylic acids, specifically TarAc-2, MalAc-2, CitAc-3 and ButAc-4. The results suggest that there was no gain in using carboxylic acids with more than two COOH-groups at the buffer concentration used for this experiment. Only samples treated with one of the monocarboxylic acids show clear shortcomings in terms of capacity retention, when compared to the group of multicarboxylic acids. Within the group of mono- and dicarboxylic acids, there are HexAc-1, AdiAc-2 and SucAc-2 with poorer capacity retention capabilities as compared to the best performing acids of their group, namely GlyAc-1, AcAc-1, MalAc-2 and TarAc-2. Compared to MalAc-2 and TarAc-2, the two samples comprising the monocarboxylic acids GlyAc-1 and AcAc-1, respectively, similar capacity fading to that of SucAc-2. While GlyAc-1 supports crosslinking through its -COOH and -OH moieties, AcAc-1 has no additional functionality to crosslink. Yet the capacity retention is on par with the samples prepared with the glycolate and succinate buffers, respectively. As evident from Scheme 1, the length of the hydrocarbon chain between two carboxylic acid groups becomes longer in the lineup: SucAc-2 < AdiAc-2 < HexAc-1. The two terminal carboxylic groups of SucAc-2 and the shorter hydrocarbon segment places of SucAc-2 in an intermediate position between the well-performing carboxylic acids with a dense number of polar moieties (TarAc-2, MalAc-2 and CitAc-3 that also contain hydroxyl-groups, see Scheme 1) and a group of more hydrophobic and poor-performing carboxylic acids. In fact, in the case of hexanoate buffer solution, the concentration had to be somewhat decreased in order to avoid phase separation. Given the A^-/HA ratio of HexAc (as well as the AdiAc-2) solution (table 2), they are unlikely to act as buffer systems. It is also possible that these compounds adsorb preferentially on the CB, rather than the silicon surface, through their hydrophobic segments.

The acid strength is reflected in the pK_a-values and the resulting base-to-acid ratio (table 2). The carboxylic acids with the highest capacity retention exhibit their first pK_a-values below 3.6 and, as a result, reach higher concentrations of the conjugate base in the buffer. However, this parameter appears to play only a secondary role, considering that Si electrodes prepared from glycolate- and formate-buffered solutions (both acids have a pK_a-value of 3.8) display significant differences in capacity retention. In fact, formic acid does stand out in this experimental series, since its physical properties (comparatively low pK_a, polar molecule with non-hydrophobic moieties) would suggest a better performance profile. A problem associated to monocarboxylic acid in particular could be their low boiling points (table 2), e.g. for ForAc and AcAc. During the drying process under reduced pressure the acids evaporate readily or decompose [27] before esterification reaction sets in. Acids with more carboxyl-groups show melting points >100 °C (table 2) and are less prone to evaporation.

Table 3. Initial Coulombic efficiencies (ICE) of buffered electrode formulations vs. a buffer-free Si electrode.

Sample	Si ref	ForAc	GlyAc	AcAc	HexAc	AdiAc
CE cycle #1	73.7%	68.0%	74.4%	79.4%	50.3%	61.6%
CE cycle #2	75.2%	81.5%	83.9%	83.3%	62.1%	67.8%
CE cycle #3	94.3%	92.4%	96.0%	96.5%	69.0%	78.8%
CE cycle #4	96.0%	93.9%	96.7%	97.4%	79.3%	82.7%
Sample	Si ref	SucAc	MalAc	TarAc	CitAc	ButAc
CE cycle #1	73.7%	69.1%	77.0%	76.6%	72.2%	74.8%
CE cycle #2	75.2%	86.0%	85.4%	84.2%	87.4%	88.5%
CE cycle #3	94.3%	96.2%	96.8%	96.1%	96.8%	96.9%
CE cycle #4	96.0%	97.4%	97.6%	96.8%	97.0%	97.7%

3.1.2. Initial Coulombic efficiencies (ICE)

Interestingly, the effect on the long term capacity retention by different carboxylic acid treatments is only partly translated into higher ICE. The ICE for the first four cycles is shown in table 3 and it is the mean Coulombic efficiency (CE) out of at least two cycling experiments per sample. The unbuffered Si electrodes show an average first cycle CE of 73.7% (±1.1%)). ForAc, HexAc and AdiAc, that displayed the poorest capacity retention among the tested buffered Si samples, show collectively lower first cycle CE's. SucAc that represented an intermediate case amongst the difunctional carboxylic acids in terms of capacity retention (figure 1(b)) also showed a lower mean first-cycle CE. That being said, there appears to be no clear trend between the long-term capacity retention and the first cycle CE (table 3), as CitAc, MalAc, TarAc and ButAc show equally good capacity retention, but their CE's range from 72.2% (CitAc) to 77.0% (MalAc). In fact, the highest CE on the first cycle was achieved by AcAc with 79.4%. After only four cycles the CE of those carboxylic acids that show clear improvements over the unbuffered electrode formulation (4th cycle CE of 96.0% ± 0.5%) on the long term lies in a narrow range between 96.7%–97.7%. The CE indicated for the unbuffered samples, the standard deviation of these values is between 0.5%–1.0%, which makes it difficult to testify clear advancement in CE of buffered electrode formulations, despite their apparent benefits in long-term performance improvements.

3.1.3. Differential capacity (dQ/dE)

An analysis of the differential capacity is provided in the *supporting information* (figures S2(a) and (b)) and was also provided in our previous work for GlyAc, MalAc and CitAc [29].

3.2. Different buffer contents

It has been shown that carboxylic acids bind readily to the Si surface [17]. In our previous study, buffer concentration of 100 mm was used [29], while other literature studies employed a higher concentrations of 173 mm [13, 25, 39]. This poses the question of how much buffer an electrode can handle before its positive effects are rendered obsolete?

For example, preliminary in-house experiments showed that citric acid is partly soluble in the carbonate electrolyte: the electrolyte solution turned into a dark brown solution within a few weeks at room temperature. The presence of citric acid, more precisely its protons, might accelerate the autocatalytic decomposition of the electrolyte salt [40] and the solvent [41, 42], including the FEC additive [43]. In addition, it has to be considered that the buffer components remain as dead weight in the electrode after drying [13, 29]. Therefore, the buffer could affect the electrode performance adversely and its concentration should be as low as possible. Being the most widely used carboxylic acid for the purpose of performance-enhancement of Si electrodes and being amongst the most effective acids (see above) a series of different citrate buffer concentrations was tested during the Si slurry preparation. Si electrodes were prepared in citrate buffer concentration range of 50–300 mm with a constant *pH* of 3. The impact of different buffer concentrations on the cycling behavior of the Si electrodes was studied and was additionally coupled with OEMS experiments in order to understand concentration effects on changes in the gas evolution behavior during both slurry preparation and SEI formation.

3.2.1. Electrode cycling in Si‖Li half cells

In figure 2(a), the measured discharge capacities are plotted as a function of cycle number for five different buffer concentrations, as stated in table 1. Corresponding voltage profiles for selected cycles are provided in figure S4. Si electrodes, prepared in buffered solutions with a concentration range of 50–200 mm, perform

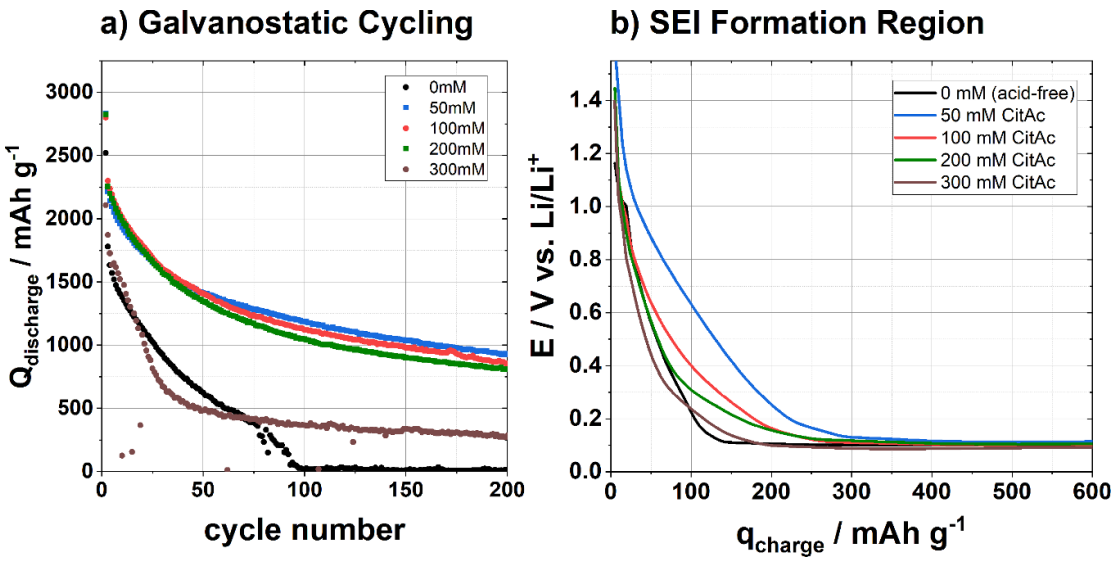

Figure 2. Specific capacity (a) and the voltage profile during 1st charge (b) of Si electrodes prepared in citrate-buffer solutions with different buffer concentrations.

collectively better in terms of capacity retention than the corresponding buffer-free electrode. The results also show an increasing capacity gap between the buffer-free and the buffer-containing samples with increasing cycle number, highlighting the fact that the capacity retention is improved due to the acid treatment during the slurry preparation. Only the Si electrode, prepared with the 300 mm buffer (Si-CitAc-300 mm), displayed a rapid capacity fading that was similar to the buffer-free sample (Si-CitAc-0 mm). The measured discharge capacity of Si-CitAc-300 mm starts to level off after ca. 30 cycles at values below 500 mAh g^{-1} and further capacity fade is slowed down significantly. The main origin of the rapid capacity fade is likely rooted in the higher mass loading of the electrode, as mentioned above [34, 35]. The slurry became much more viscous as the buffer concentration was raised from 200 mm to 294 mm, yielding higher mass loadings for this formulation.

We have found previously that samples containing MalAc and CitAc showed more irreversible charge during the SEI formation process than a buffer-free electrode, which translated into a better capacity retention on the long term [29]. The analogous comparison is shown in figure 2(b) for voltage profiles of the five formulation with different citric-acid-buffer contents in the SEI formation region on the first charge. Here, the formulation with the lowest buffer content, the 50 mm-formulation, showed the largest irreversible loss, while the voltage drops faster in samples with a higher buffer content. As the buffer content increases, the voltage profile becomes more similar to the one of the buffer-free electrode. For example, the 200 mm-formulation deviates from the voltage profile of the 0 mm-formulation only below a potential of 400 mV vs. Li$^+$/Li, while for the 50 mm-formulation it coincides only at cut-off potential. Regarding the capacity retention of the half-cells, it appears that up to the critical limit in the concentration range between 200 to 294 mm any acid amount will provide about the same improvement and only excessive acid contents cause drastic capacity losses.

Using the dQ/dE maps for this set of samples (figures S3(a) and (b)), it can be readily seen that the Si-CitAc-52 mm sample shows the longest signature for the delithiation reaction at lower potentials, just below 400 mV *vs* Li$^+$/Li, as well as for the first lithiation reaction above 200 mV *vs* Li$^+$/Li. The result suggests that this formulation is the most reversible among the five tested. In comparison, Si-CitAc-100 mm and Si-CitAc-200 mm show a faster fading of the dQ/dE signals. Because of the rapid fading of Si-CitAc-0 mm and Si-CitAc-294 mm, the dQ/dE data are very scattered and thus provide little useful information. It is worth mentioning though that Si-CitAc-294 mm electrode shows high dQ/dE values around the first lithiation stage over the first 20 cycles, same as the other buffer-containing formulations, whereas this feature is essentially absent in buffer-free electrodes and only visible for a couple of cycles. The Si-CitAc-0 mm cell operates predominantly between the second reaction step upon lithiation and the first reaction step upon delithiation (i.e. it is confined to a narrower potential window), which also limits the charge that can be extracted from the electrode.

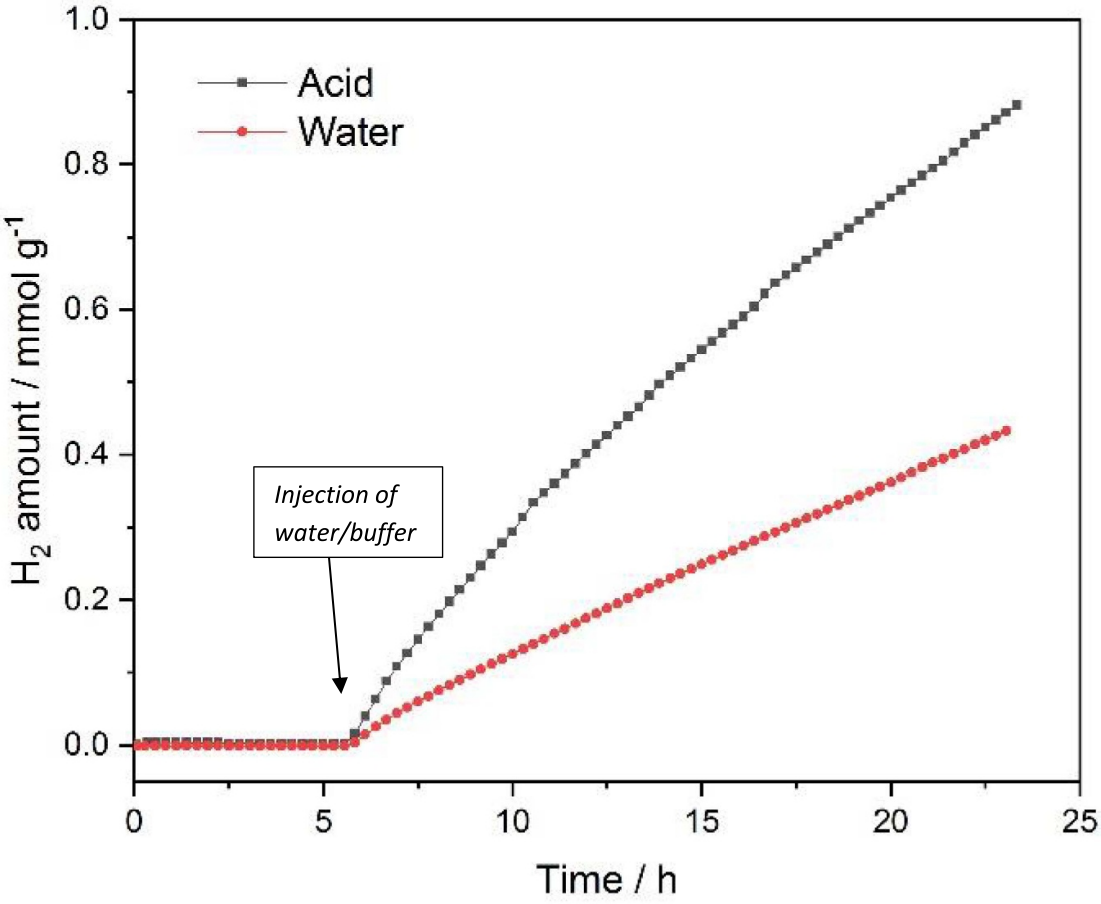

Figure 3. Comparison of released H_2 amounts from titration experiments where Si nanoparticles are reacted with either water or citrate buffer.

3.2.2. Gas evolution during slurry preparation

Another process that contributes to the changes of the Si surface during the carboxylic-acid-treatment is the hydrogen evolution from Si particles in contact with H_2O and acid [44–47]. The reaction rate at room temperature is particle-size- and *pH*-dependent [45, 46], leading to a notable H_2 evolution when nanoparticles are used. A semi-closed system connected to a mass spectrometer was used in our study to track and quantify the gas evolution during the process of Si exposure to either water or buffer.

Two hundred microliter of either deionized water or citrate buffer solution (100 mm, $pH = 3$) was injected into a cell, where ca. 10 mg of nano-sized Si powder was placed beforehand. While H_2 continuously evolves throughout our measurement interval (figure 3), the H_2 amount was doubled when citrate buffer was injected as compared to H_2O exposure.

It is worth mentioning that in a previous study by Rodrigues *et al* [45], silicon immersed in deionized water produced slightly more hydrogen than an aqueous solution of PAA, while we observed the opposite trend in our experiments. However, the authors in [45] also showed that partly deprotonated PAA (in their study 20% deprotonation, $pH = 4.5$) causes increased H_2 gas evolution beyond the levels of deionized water samples. Although our buffer solution is at $pH = 3$, the acid-to-conjugated-base ratio is approximately the same (18%, table 2). This poses new questions about the role of the conjugated base in this process. Following the Pourbaix diagram, as suggested by Nikolaychuck [48], soluble $SiO_{2,(aq)}$ as well as meta- and orthosilicic acid (H_3SiO_3 and H_4SiO_4) are formed at low *pH* during formation of H_2. This would be in accordance with earlier findings by Touidjine *et al* [44], who observed the formation of porosity within the otherwise dense and protective native $SiO_{2,(s)}$ layer on a bulk Si as soon as the particles are brought into contact with water.

Based on previous observations [44], these results suggest that the Si particle surface changes on the influence of the citrate buffer during the preparation of the Si slurry. Any change of the surface properties potentially affects the electrochemistry of the electrode, which will be reflected in parameters such as the initial discharge capacity or capacity retention [44]. In a sole presence of an aqueous CMC-Na solution

Table 4. Si electrodes for OEMS study.

Sample	Buffer conc./mM	Buffer volume[a]/ml	Buffer amount[b]/ mg (wt.%)	Effective Si content/wt.%	Si (total) loading/ mg cm^{-2}
Buffer-0 mm	0	0	0 (0 wt.%)	79.8	2.29 (2.87)
Buffer-100 mm	100	4.47	102.6 (9.2 wt.%)	72.8	2.35 (3.22)
Buffer-200 mm	200	4.47	202.2 (16.8 wt.%)	66.4	2.22 (3.34)

[a] buffer volume for 1 g of solid electrode components.
[b] referred to the total buffer volume per slurry.

($pH \approx 7$), the dissolution of the native SiO_2 layer slows down and at pH-values > 7, i.e. in the presence of OH^-, the dissolution proceeds the fastest, forming soluble silicates (e.g. $H_3SiO_4^-$, $H_2SiO_4^{2-}$) and H_2 as byproduct [45].

3.2.3. Gas evolution during cycling

As reported previously, the carboxylic acid shows strong interactions with the Si surface [16, 17, 29]. Its presence affects the SEI layer composition [16] and reduces the electrode expansion by improving the mechanical properties [39] of the electrode, such as hardness and elastic modulus. In addition, Lucht and co-workers also showed that the SEI layer composition changes in presence of carboxylic acids [16]. These changes are reflected also in our data, for instance in the voltage profiles of the SEI formation region shown in figure 2(b). Any involvement of the carboxylic acid in the SEI layer formation should also be visible in the quantities of gaseous byproducts during the SEI formation. Therefore, OEMS was employed, for the first time, to analyze the passivation process of citrate-treated Si electrodes in *operando*. A buffer-free electrode served as reference (denoted as Buffer-0 mm), and two formulations with 100 and 200 mm of citrate buffer solutions (Buffer-100 mm and Buffer-200 mm, respectively) were analyzed. As the electrode slurries for this experiment were cast on copper mesh, the slurry viscosity had to be adjusted and, therefore, the amounts of buffer in the electrode (table 4) are slightly higher than those for the formulations stated in table 1.

Figure 4 compares the gassing of Buffer-0 mm, Buffer-100 mm, and Buffer-200 mm samples during two cycles of CV measurements. A more detailed view on the CV data can be found in figures S5(a) and (b), where current-time transients were replotted as typical I vs. E plots separately for both cycles. Figure S5(a) also contains an enlarged inset for the SEI formation region. In general, the corresponding cyclic voltammograms are in good agreement with the differential capacity (dQ/dE) plots in figures S3(a) and (b), validating the legitimacy of the CV measurements. It is worth mentioning that systematic error may arise in determining the correct mass loading, hence the normalized gassing data of Si electrodes. A notable mass variation was identified, when weighing individual discs punched out of a 75 μm-thick Cu mesh. Extended comparison of bare Cu mesh discs and coated electrodes is presented in figures S5(c) and (d). This is a known issue that has been previously described for Si electrodes [8], since the Cu substrate is significantly heavier than the electrode coating and can readily lead to over- or underestimation of the active electrode mass. To minimize its impact, each sample was repeated at least three times, and all results were included in the supporting information for comparison (figures S5(e)–(g)). All electrodes from the same sample show same gassing features and only vary slightly in intensity.

3.2.4. Hydrogen (H_2) evolution

H_2 evolves in three stages in the first cycle. In Stage I, Buffer-100 mm and Buffer-200 mm first evolve H_2 when the potential is negatively swept between ca. 2.3–1.5 V. A peak is also observed in the 1st-cycle CV plot (figure S5(a)), corresponding to the electrochemical reduction of protic species (equation (1)) in the electrolyte, such as H_2O and ROH (equations (2) and (3)) [30, 49–52]:

$$2H^+ + 2e^- \rightarrow H_2 \uparrow \quad (1)$$

$$2H_2O + 2e^- \rightarrow 2OH^- + H_2 \uparrow \quad (2)$$

$$2ROH + 2e^- \rightarrow 2RO^- + H_2 \uparrow . \quad (3)$$

Strikingly, such a H_2 peak is omitted in the potential range in the control experiment (Buffer-0 mm). Therefore, it is believed that the first H_2 evolution process is linked to protic species brought in to the cell by the citrate buffer solution, possibly in the form of trace dissociated protons or citrate hydrates. The evolved

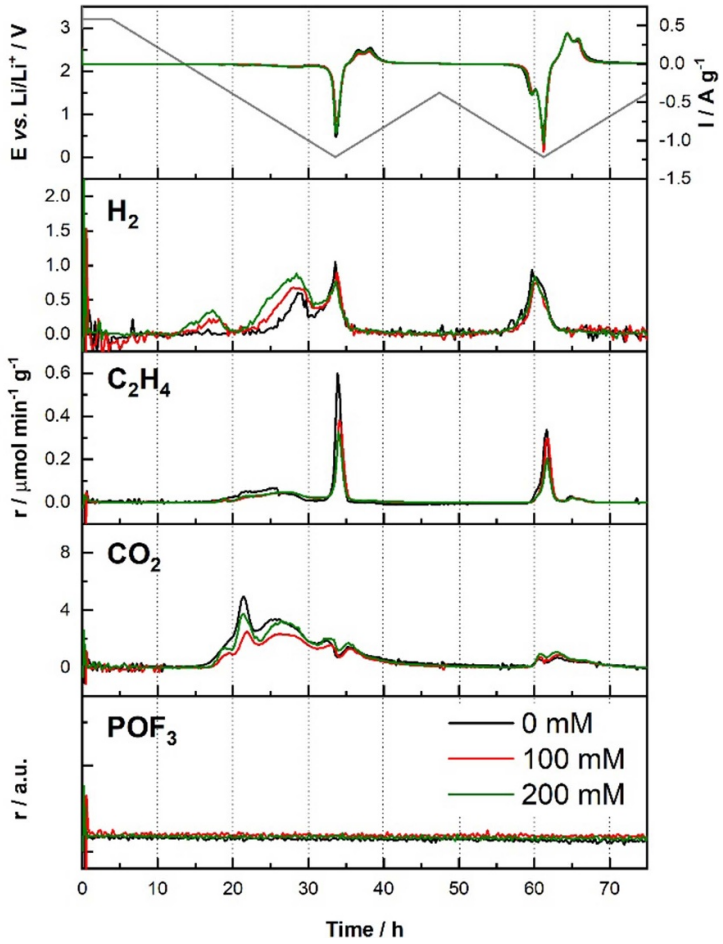

Figure 4. OEMS measurements summarizing the impact of citrate buffer solutions on the gassing of Si anodes in the first two cycles of cyclic voltammetry tests. Solutions without acid (black line), with 100 mm (red line) and 200 mm (green line) of the acid were quantitatively compared.

H_2 amount also positively correlates to the concentration of the buffer solution, i.e. the amount of H_2 released by Buffer-200 is 135.7% that of the Buffer-100.

The second stage of H_2 evolution occurs, when the potential is further swept between 1.3–0.3 V. The broad H_2 peak is indicative of a collection of different reduction processes, all contributing to the H_2 gassing during SEI formation and 1st lithiation. The amount of H_2 released by Buffer-200 mm continues to scale with the buffer concentration, being 141.4% and 239.5% that of the Buffer-100 mm and Buffer-0 mm, respectively.

In the last stage of H_2 evolution, namely when the potential is lower than 0.3 V (both during 1st lithiation and 1st de-lithiation), a sharp peak with approximately equal amount of H_2 is observed for all three samples. In addition, this peak shows up again in the second CV cycle, when the potential is lower than 0.6 V in the 2nd lithiation and lower than 0.3 V in the 2nd de-lithiation.

3.2.5. Ethylene (C_2H_4) evolution

C_2H_4 is a typical by-product accompanying the ethylene carbonate (EC) electrochemical reduction (equation (4)):

$$C_3H_4O_3 + Li^+ + e^- \rightarrow 1/2(CH_2OCOOLi)_2 + C_2H_4 \uparrow . \quad (4)$$

In the presence of FEC, a film-forming additive, the extent of EC reduction is significantly suppressed, with merely marginal C_2H_4 formation between 1.7–0.3 V. In addition, alike H_2, a distinct C_2H_4 peak is identified in both CV cycles, hinting that new interphases are forming towards the end of lithiation. Dilatometry results by Tranchot *et al* [39] indicate a steep increase in electrode thickness in this last region of the alloying process of Si. Hence, the peak is likely a result of SEI fracture and re-formation during Si particle expansion upon the alloying reaction. Concerning the buffer solutions, both Buffer-100 mm and

Buffer-200 mm release 32.5% less C_2H_4 than Buffer-0 mm, suggesting the citrate buffer better-passivating the surface of Si nanoparticles.

3.2.6. Carbon dioxide (CO_2) evolution

The CO_2 profile presents multiple overlapping peaks, signifying the complexity of the cell chemistry. Among various possibilities, typical CO_2 source includes the Lewis-base-assisted ring-opening of EC (equation (5)) and the electrochemical reduction of FEC (equation (6)):

$$C_3H_4O_3 + OH^- \rightarrow C_2H_5O_2^- + CO_2 \uparrow \quad (5)$$

$$C_3H_3O_3F + Li^+ + e^- \rightarrow CH_2CHO + LiF + CO_2 \uparrow . \quad (6)$$

The CO_2 first evolves as a minor shoulder peak at ca. 1.8 V, which coincides with the maximum H_2 evolution rate. Therefore, it is reasonable to assume that the CO_2 evolution is triggered by the OH^-–assisted ring-opening of EC. Afterwards, the main CO_2 peak, centered around 1.3 V, agrees with the widely reported FEC reduction potential and can be unambiguously assigned to the SEI formation process. Note that CO_2 continues evolving till the end of the 1st lithiation, which agrees with our recent assessment on the gassing of FEC in Na-ion cells [53]. Furthermore, trace CO_2 evolution is also identified during the 1st de-lithiation, when the potential is below ca. 0.8 V. Jung *et al* assigned this behavior to the reduction of FEC at the Li counter electrode [54].

It is worth commenting that, although the citrate buffer solution introduces massive—COOH groups to the Si surface, higher citrate concentration does not result in more CO_2 release. In contrast, slightly less CO_2 is observed for Buffer-100 mm and Buffer-200 mm, re-confirming that the presence of citrate buffers alters the surface chemistry of Si nanoparticles, hence changing the SEI composition.

3.2.7. Phosphoryl trifluoride (POF_3) evolution

One of the fundamental questions we have aimed to answer by OEMS was the impact of the high concentration of protons on the electrolyte salt decomposition. POF_3 gas evolution can be used as an indicator for $LiPF_6$ salt decomposition (equation (7)), as previously reported [55]. Recently, it was shown by Solchenbach *et al* [56] that addition of a proton source, such as methanesulfonic acid (MSA), to the electrolyte resulted in the formation of considerable PF_5 and POF_3 (equations (8) and (9)). Degraded electrolyte salt species can trigger the autocatalytic (chemical) decomposition of electrolyte components [42]. Particularly, HF is problematic in regards to Si electrodes, as it etches the native Si oxide layer [2, 8]:

$$LiPF_6 + H_2O \rightarrow LiF + 2HF + POF_3 \uparrow \quad (7)$$

$$LiPF_6 + H^+ \rightarrow Li^+ + HF + PF_5 \uparrow \quad (8)$$

$$PF_5 + H_2O \rightarrow 2HF + POF_3 \uparrow . \quad (9)$$

Nevertheless, irrespective of the huge amount of proton brought into the system by the acid buffer, no POF_3 signal was detected. We argue that, unlike MSA, carboxylic acids show considerably smaller dissociation constants in aprotic media than in water. For example, the pK_a value of acetic acid increases from 4.8 (H_2O) to 12.3 in DMSO and to 22.3 in Acetonitrile [57]. For comparison, the pK_a of MSA increases from −0.6 in H_2O to only 1.6 in DMSO [58]. In accordance to the OEMS results, it can thus be assumed that the carboxylic acids remain associated with their protons, which could prevent any significant electrolyte salt decomposition induced by free protons. Later on, protons may be reduced during the SEI formation, or removed by other (electro)chemical reactions, in agreement with the Stage I & II of the H_2 formation process.

3.2.8. Summary

Having scrutinized individual gassing contributions, it is evident that the presence of surface carboxylate functional groups is beneficial to stabilize the surface of Si nanoparticles and minimize the electrolyte consumption during SEI formation. Extra H_2 is only detected in the 1st cycle from samples treated with citrate buffer solution, while none of the protons end up reacting with the $LiPF_6$ salt and destabilizing the system. The SEI formation can thus been summarized in the following steps:

(1) When the potential is negatively swept between 2.3–1.5 V *vs.* Li/Li^+, trace dissociated protons or citrate hydrates are first reduced, forming H_2 in Buffer-100 mm and Buffer-200 mm (equations (1)–(3)).

(2) The Lewis bases (OH^-, ROH^-, etc) decompose carbonate solvents into trace CO_2 following a catalytic ring-opening reaction path (equation (5)).
(3) Since carboxylate functional groups reside on the surface of Si nanoparticles, the electrochemical reduction of FEC around 1.3 V (equation (6) is mitigated in Buffer-100 mm and Buffer-200 mm. The reduction of EC remains insignificant (equation (4)).
(4) When the potential is close to the lower cut-off potential (0.005 V *vs.* Li/Li^+), Si particle expansion during the alloying process may result in SEI fracture and create new interphases. The SEI re-formation is identified from a gassing perspective.
(5) Despite that massive amounts of protons in the form of—COOH is introduced to the electrode composites, POF_3 gas is not observed as a possible electrolyte degradation product, reassuring the improved stability of citrate-treated electrodes.

3.2.9. Different types of carboxylic acid

We have demonstrated that electrode-performance improvements due to use of carboxylic acid buffers are observed across the experimental series, independent of the number of functional groups, even though monocarboxylic acids appear to perform slightly worse than carboxylic acids with more carboxyl groups, in agreement with our previous results [29]. Figure 1 implies that at least two carboxyl groups are required to maximize the capacity retention of the Si electrodes, as among carboxylic acids with two or more functional groups, there was little difference in terms of their impact on capacity retention. Although the acidity itself might not play a decisive role, low pK_a-values do indicate polar compounds with a dense number of functional groups (e.g. TarAc vs. SucAc). Larger hydrophobic segments as in HexAc and AdiAc seem to affect the cyclability of the Si electrodes adversely. The reason for this can be that they render the Si surface more hydrophobic, which could compromise the interaction with the (hydrophilic) CMC-Na binder or alter the SEI layer formation. Furthermore, it is more likely that longer hydrophobic segments show stronger adsorption on CB.

As mentioned in the introduction, several effects are taking place in parallel during slurry preparation and cycling: binder crosslinking, surface adsorption/tethering, binder grafting and changes in the general particle distribution, as well as during cycling sacrificial decomposition of the carboxylic acids and 'artificial-SEI'-type properties may influence the surface layer properties. An analysis of the SEI layer for example by x-ray photoelectron spectroscopy is beyond the scope of this work, but could be useful to understand the electrode interfaces in these systems in greater detail.

3.2.10. Different buffer contents

The results highlight that acidic protons from the carboxylic acid treatment undergo an early reduction reaction, prior to the decomposition of FEC (1.3 V vs. Li/Li^+). The amount of produced hydrogen scales with the buffer content in the electrode, which can be understood in terms of citric acid surface coverage on Si and carbon black particles. After the surface is saturated with adsorbed species, 'free acid' (i.e. not adsorbed) remains in the electrode and thus increases the concentration of acidic protons that are potentially prone to chemical or electrochemical side reactions. Given the significant increase in the H_2 evolution rate from a Si electrode prepared in a 200 mm citrate buffer to the one prepared in a 100 mm citrate buffer, it is reasonable to assume that 'excess amounts' of citric acid in the electrode is the main origin of the increased gassing rate. Therefore, the proton concentration in the final electrode could be considerably smaller than anticipated from the initial amounts of acid in the buffer solution, because of the hydrogen evolution reaction of Si (figure 3) in acidic aqueous media [45] and reactions between carboxylic acids and binder during slurry preparation and electrode drying (i.e. esterification and cross-linking) [19, 59]. The amount of protons that are consumed by these reaction pathways is consequently also a function of the nanoparticle surface area and the surface reactivity, which is intrinsically particle-size dependent [46]. Therefore, it is not so surprising that the reduction reaction of the 'free acid' is less prominent in the 100 mm- than in the 200 mm-formulation, where the potential excess of protons is larger. With the H_2 evolution on the first cycle, protons are effectively removed before they can induce adverse side reactions with the electrolyte solvents, additives or salt. The resulting carboxylates after the reductive deprotonation can be considered relatively stable towards reduction in aprotic solvents [60], which is supported for example by a smaller CO_2 evolution.

Reduction reactions of carboxylic acids (yielding aldehydes or alcohols) usually require strong reducing agents, such as hydrides or alkali metal [61] (as in a Bouveault-Blanc-type reaction). This is in general agreement with the IR and XPS findings by Nguyen and Lucht [62], who concluded that Li-citrate is a major component of the SEI that stabilizes the Si surface. In fact, as seen in the CO_2 evolution rate in the FEC reduction region, the FEC consumption is notably reduced as compared to buffer-free electrodes. Lastly, proton-induced parasitic side reactions that would be indicated by the formation of electrolyte-salt degradation products, e.g. POF_3, where not detected by OEMS. Based on previous literature on the pK_a

values in aprotic media, the carboxylic acids show presumably very small degrees of dissociation and a significant fraction of these protons appears to be removed as hydrogen before the SEI formation commences (figure 4).

4. Conclusions

In this work, carboxylic acids with different molecular weights and numbers of functional groups were investigated for their use as buffers in the preparation of Si electrodes via low-*pH* slurries. Herein, we showed that the concept from often-used citrate buffers can be extended to carboxylic acids, which contain at least two carboxyl groups and have a low pK_a values. Carboxylic acids with longer hydrophobic-chain segments do not provide the same kind of improvements in terms of capacity retention and can even accelerate capacity fading, answering the first question raised in this study. The results demonstrated that the absolute buffer content in the final electrode composite can reach surprisingly high levels of at least 18 wt.% before the capacity retention is notably affected, as in 200 mm of citrate buffer. Conversely, the buffer content can be chosen as low as 5 wt.% (and possibly even lower) without making any sacrifices with respect to capacity retention, as in 50 mm of citrate buffer. A minimal amount needed for performance improvement is desirable, as reducing the inactive material content of the electrode formulations leads to higher specific energy of the cell. With respect to the second question, we have shown that the buffer concentration can be varied in a broad range between 50–200 mm with no impact on capacity retention, although an optimal value has not been established.

An OEMS analysis on buffer-containing Si electrodes was conducted in order to understand the role of protons within a buffer onto the SEI formation, answering the last question, raised in this study. We have correlated various gas evolution phenomena to the SEI formation process, and showed that less electrolyte species, in particular FEC and EC, are consumed in the presence of citrate buffers. In addition, no adverse effects could be noted from high acidic proton contents in buffer-containing electrode formulations. Instead, we confirm that the protons are electrochemically removed upon 1st lithiation prior to any SEI formation process in the potential regions between 2.3–1.5 V *vs.* Li/Li^+, and the H_2 evolution rate in first cycle scales with the buffer content. Several processes during the slurry preparation were also identified to consume protons, yielding H_2 or H_2O, rendering the effective proton concentration in the final electrode lower than inferring from the original buffer concentration. Any excess of protons then reacts in the initial stage of the first lithiation. Furthermore, proton-induced electrolyte salt decomposition was not observed either.

Data availability statement

The data that support the findings of this study are available upon reasonable request from the authors.

Acknowledgments

The authors would like to thank Dr Christoph Bolli for fruitful discussions on the OEMS results. F S would like to thank the IAESTE exchange program for the opportunity to conduct an internship at PSI. F J and S T acknowledge financial support by Innosuisse (Project No. 18254.2).

ORCID iDs

Fabian Jeschull https://orcid.org/0000-0002-5927-1978
Leiting Zhang https://orcid.org/0000-0003-4057-7106
Łukasz Kondracki https://orcid.org/0000-0002-2489-9394
Sigita Trabesinger https://orcid.org/0000-0001-5878-300X

References

[1] Obrovac M N and Chevrier V L 2014 Alloy negative electrodes for Li-ion batteries *Chem. Rev.* **114** 11444–502
[2] Philippe B, Dedryvère R, Gorgoi M, Rensmo H, Gonbeau D and Edström K 2013 Role of the LiPF 6 salt for the long-term stability of silicon electrodes in Li-ion batteries—a photoelectron spectroscopy study *Chem. Mater.* **25** 394–404
[3] Oumellal Y, Delpuech N, Mazouzi D, Dupré N, Gaubicher J, Moreau P, Soudan P, Lestriez B and Guyomard D 2011 The failure mechanism of nano-sized Si-based negative electrodes for lithium ion batteries *J. Mater. Chem.* **21** 6201
[4] Nguyen B P N, Gaubicher J and Lestriez B 2014 Analogy between electrochemical behaviour of thick silicon granular electrodes for lithium batteries and fine soils micromechanics *Electrochim. Acta* **120** 319–26
[5] Lindgren F, Xu C, Maibach J, Andersson A M, Marcinek M, Niedzicki L, Gustafsson T, Björefors F and Edström K 2016 A hard x-ray photoelectron spectroscopy study on the solid electrolyte interphase of a lithium 4,5-Dicyano-2-(Trifluoromethyl)Imidazolide based electrolyte for Si-electrodes *J. Power Sources* **301** 105–12

[6] Buqa H, Holzapfel M, Krumeich F, Veit C and Novák P 2006 Study of styrene butadiene rubber and sodium methyl cellulose as binder for negative electrodes in lithium-ion batteries *J. Power Sources* **161** 617–22
[7] Hochgatterer N S, Schweiger M R, Koller S, Raimann P R, Wöhrle T, Wurm C and Winter M 2008 Silicon/graphite composite electrodes for high-capacity anodes: influence of binder chemistry on cycling stability *Electrochem. Solid State Lett.* **11** A76
[8] Jeschull F, Lindgren F, Lacey M J, Björefors F, Edström K and Brandell D 2016 Influence of inactive electrode components on degradation phenomena in nano-Si electrodes for Li-ion batteries *J. Power Sources* **325** 513–24
[9] Erk C, Brezesinski T, Sommer H, Schneider R and Janek J 2013 Toward silicon anodes for next-generation lithium ion batteries: a comparative performance study of various polymer binders and silicon nanopowders *ACS Appl. Mater. Interfaces* **5** 7299–307
[10] Magasinski A, Zdyrko B, Kovalenko I, Hertzberg B, Burtovyy R, Huebner C F, Fuller T F, Luzinov I and Yushin G 2010 Toward efficient binders for Li-ion battery Si-based anodes: polyacrylic acid *ACS Appl. Mater. Interfaces* **2** 3004–10
[11] Mazouzi D, Karkar Z, Hernandez C R, Manero P J, Guyomard D, Roué L and Lestriez B 2015 Critical roles of binders and formulation at multiscales of silicon-based composite electrodes *J. Power Sources* **280** 533–49
[12] Mazouzi D, Lestriez B, Roué L and Guyomard D 2009 Silicon composite electrode with high capacity and long cycle life *Electrochem. Solid State Lett.* **12** A215–8
[13] Delpuech N *et al* 2014 Critical role of silicon nanoparticles surface on lithium cell electrochemical performance analyzed by FTIR, Raman, EELS, XPS, NMR, and BDS spectroscopies *J. Phys. Chem.* C **118** 17318–31
[14] Karkar Z, Guyomard D, Roué L and Lestriez B 2017 A comparative study of polyacrylic acid (PAA) and carboxymethyl cellulose (CMC) binders for Si-based electrodes *Electrochim. Acta* **258** 1–14
[15] Maver U, Znidarsic A and Gaberšček M 2011 An attempt to use atomic force microscopy for determination of bond type in lithium battery electrodes *J. Mater. Chem.* **21** 4071
[16] Nguyen C C, Seo D M, Chandrasiri K W D K and Lucht B L 2017 Improved cycling performance of a Si nanoparticle anode utilizing citric acid as a surface-modifying agent *Langmuir* **33** 9254–61
[17] Chandrasiri K W D K, Nguyen C C, Parimalam B S, Jurng S and Lucht B L 2018 Citric acid based pre-SEI for improvement of silicon electrodes in lithium ion batteries *J. Electrochem. Soc.* **165** A1991–6
[18] Bresser D, Buchholz D, Moretti A, Varzi A and Passerini S 2018 Alternative binders for sustainable electrochemical energy storage-the transition to aqueous electrode processing and bio-derived polymers *Energy Environ. Sci.* **11** 3096–127
[19] Kazzazi A, Bresser D, Birrozzi A, Zamory Von J, Hekmatfar M and Passerini S 2018 Comparative analysis of aqueous binders for high-energy Li-Rich NMC as lithium-ion cathode and the impact of adding phosphoric acid *ACS Appl. Mater. Interfaces* **10** 17214–22
[20] Song J, Yu Z, Gordin M L, Li X, Peng H and Wang D 2015 Advanced sodium ion battery anode constructed via chemical bonding between phosphorus, carbon nanotube, and cross-linked polymer binder *ACS Nano* **9** 11933–41
[21] Pang Q, Liang X, Kwok C Y, Kulisch J and Nazar L F 2017 A comprehensive approach toward stable lithium–sulfur batteries with high volumetric energy density *Adv. Energy Mater.* **7** 1–9
[22] Koo B, Kim H, Cho Y, Lee K T, Choi N-S and Cho J 2012 A highly cross-linked polymeric binder for high-performance silicon negative electrodes in lithium ion batteries *Angew. Chem., Int. Ed.* **51** 8762–7
[23] Vanpeene V, Villanova J, King A, Lestriez B, Maire E and Roué L 2019 Dynamics of the morphological degradation of Si-based anodes for Li-ion batteries characterized by *In Situ* synchrotron x-ray tomography *Adv. Energy Mater.* **1803947** 1803947
[24] Hernandez C R, Etiemble A, Douillard T, Mazouzi D, Karkar Z, Maire E, Guyomard D, Lestriez B and Roué L 2018 A facile and very effective method to enhance the mechanical strength and the cyclability of Si-based electrodes for Li-ion batteries *Adv. Energy Mater.* **8** 1–13
[25] Reale Hernandez C, Karkar Z, Guyomard D, Lestriez B and Roué L 2015 A film maturation process for improving the cycle life of Si-based anodes for Li-ion batteries *Electrochem. Commun.* **61** 102–5
[26] Mazouzi D, Grissa R, Paris M, Karkar Z, Huet L, Guyomard D, Roué L, Devic T and Lestriez B 2019 CMC-citric acid Cu(II) cross-linked binder approach to improve the electrochemical performance of Si-based electrodes *Electrochim. Acta* **304** 495–504
[27] Wei C and Obrovac M N 2019 Small molecule slurry additives for Si alloy coatings with CMC/SBR binder *J. Electrochem. Soc.* **166** A3217–21
[28] Nguyen B P N, Chazelle S, Cerbelaud M, Porcher W and Lestriez B 2014 Manufacturing of industry-relevant silicon negative composite electrodes for lithium ion-cells *J. Power Sources* **262** 112–22
[29] Jeschull F, Scott F and Trabesinger S 2019 Interactions of silicon nanoparticles with carboxymethyl cellulose and carboxylic acids in negative electrodes of lithium-ion batteries *J. Power Sources* **431** 63–74
[30] Metzger M, Strehle B, Solchenbach S and Gasteiger H A 2016 Origin of H_2 evolution in LIBs: H_2O reduction vs. electrolyte oxidation *J. Electrochem. Soc.* **163** A798–809
[31] Peng H-J 2016 Unravelling the cell ageing phenomona in aprotic lithium-nickel-cobalt-manganese-oxide batteries *PhD Thesis* ETH Zürich (https://doi.org/10.3929/ethz-a-010793448)
[32] He M 2016 Elucidating interface reactions in Li-ion batteries and supercapacitors by *in situ* gas analysis *PhD Thesis* ETH Zürich (https://doi.org/10.3929/ethz-a-010852357)
[33] John R 2019 Section 5: thermochemistry, kinetics, electrochemistry, and solution chemistry *CRC—Handbook of Chemistry and Physics* (Boca Raton, FL: CRC Press)
[34] Karkar Z, Mazouzi D, Hernandez C R, Guyomard D, Roué L and Lestriez B 2016 Threshold-like dependence of silicon-based electrode performance on active mass loading and nature of carbon conductive additive *Electrochim. Acta* **215** 276–88
[35] Karkar Z, Guyomard D, Roué L and Lestriez B 2017 A comparative study of polyacrylic acid (PAA) and carboxymethyl cellulose (CMC) binders for Si-based electrodes *Electrochim. Acta* **258** 453–66
[36] Karkar Z, Jaouhari T, Tranchot A, Mazouzi D, Guyomard D, Lestriez B and Roué L 2017 How silicon electrodes can be calendered without altering their mechanical strength and cycle life *J. Power Sources* **371** 136–47
[37] Baunach M, Jaiser S, Schmelzle S, Nirschl H, Scharfer P and Schabel W 2016 Delamination behavior of lithium-ion battery anodes: influence of drying temperature during electrode processing *Dry. Technol.* **34** 462–73
[38] Jeschull F, Brandell D, Wohlfahrt-Mehrens M and Memm M 2017 Water-soluble binders for lithium-ion battery graphite electrodes: slurry rheology, coating adhesion, and electrochemical performance *Energy Technol.* **5** 2108–18
[39] Tranchot A, Idrissi H, Thivel P X and Roué L 2016 Impact of the slurry PH on the expansion/contraction behavior of silicon/carbon/carboxymethylcellulose electrodes for Li-ion batteries *J. Electrochem. Soc.* **163** A1020–6
[40] Plakhotnyk A V, Ernst L and Schmutzler R 2005 Hydrolysis in the system $LiPF_6$—propylene carbonate—dimethyl carbonate—H_2O *J. Fluor. Chem.* **126** 27–31

[41] Lux S F, Chevalier J, Lucas I T and Kostecki R 2013 HF formation in $LiPF_6$-based organic carbonate electrolytes *ECS Electrochem. Lett.* **2** A121–3
[42] Campion C L, Li W and Lucht B L 2005 Thermal decomposition of LiPF[Sub 6]-based electrolytes for lithium-ion batteries *J. Electrochem. Soc.* **152** A2327
[43] Xu C, Hernández G, Abbrent S, Kobera L, Konefal R, Brus J, Edström K, Brandell D and Mindemark J 2019 Unraveling and mitigating the storage instability of fluoroethylene carbonate-containing LiPF 6 electrolytes to stabilize lithium metal anodes for high-temperature rechargeable batteries *ACS Appl. Energy Mater.* **2** 4925–4935
[44] Touidjine A, Morcrette M, Courty M, Davoisne C, Lejeune M, Mariage N, Porcher W and Larcher D 2015 Partially oxidized silicon particles for stable aqueous slurries and practical large-scale making of Si-based electrodes *J. Electrochem. Soc.* **162** A1466–75
[45] Rodrigues M T F, Trask S E, Shkrob I A and Abraham D P 2018 Quantifying gas generation from slurries used in fabrication of Si-containing electrodes for lithium-ion cells *J. Power Sources* **395** 289–94
[46] Erogbogbo F, Lin T, Tucciarone P M, Lajoie K M, Lai L, Patki G D, Prasad P N and Swihart M T 2013 On-demand hydrogen generation using nanosilicon: splitting water without light, heat, or electricity *Nano Lett.* **13** 451–6
[47] Xu L, Ashraf S, Hu J, Edwards P P, Jones M O, Hadzifejzovic E and Foord J S 2016 Ball-Milled Si powder for the production of H_2 from water for fuel cell applications *Int. J. Hydrog. Energy* **41** 12730–7
[48] Nikolaychuk P A 2014 The revised pourbaix diagram for silicon *Silicon* **6** 109–16
[49] Metzger M, Strehle B, Solchenbach S and Gasteiger H A 2016 Hydrolysis of ethylene carbonate with water and hydroxide under battery operating conditions *J. Electrochem. Soc.* **163** A1219–25
[50] Kitz P G, Lacey M J, Novák P and Berg E J 2019 Operando EQCM-D with simultaneous *in Situ* EIS: new insights into interphase formation in Li ion batteries *Anal. Chem.* **91** 2296–303
[51] Joho F, Rykart B, Imhof R, Novák P, Spahr M E and Monnier A 1999 Key factors for the cycling stability of graphite intercalation electrodes for lithium-ion batteries *J. Power Sources* ***81–82*** 243–7
[52] Bernhard R, Metzger M and Gasteiger H A 2015 Gas evolution at graphite anodes depending on electrolyte water content and SEI quality studied by on-line electrochemical mass spectrometry *J. Electrochem. Soc.* **162** A1984–9
[53] Zhang L, Tsolakidou C, Mariyappan S, Tarascon J M and Trabesinger S 2021 Unraveling gas evolution in sodium batteries by online electrochemical mass spectrometry *Energy Storage Mater.* **42** 12–21
[54] Jung R, Metzger M, Haering D, Solchenbach S, Marino C, Tsiouvaras N, Stinner C and Gasteiger H A 2016 Consumption of fluoroethylene carbonate (FEC) on Si-C composite electrodes for Li-ion batteries *J. Electrochem. Soc.* **163** A1705–16
[55] Bolli C, Guéguen A, Mendez M A and Berg E J 2019 Operando monitoring of F—formation in lithium ion batteries *Chem. Mater.* **31** 1258–67
[56] Solchenbach S, Metzger M, Egawa M, Beyer H and Gasteiger H A 2018 Quantification of PF_5 and POF_3 from side reactions of LiPF 6 in Li-ion batteries *J. Electrochem. Soc.* **165** A3022–8
[57] Kim H-S, Chung T D and Kim H 2001 Voltammetric determination of the PKa of various acids in polar aprotic solvents using 1,4-benzoquinone *J. Electroanal. Chem.* **498** 209–15
[58] Bordwell F G 1988 Equilibrium acidities in dimethyl sulfoxide solution *Acc. Chem. Res.* **21** 456–63
[59] Kuenzel M, Bresser D, Diemant T, Carvalho D V, Kim G T, Behm R J and Passerini S 2018 Complementary strategies toward the aqueous processing of high-voltage $LiNi_{0.5}Mn_{1.5}O_4$ Lithium-ion cathodes *ChemSusChem* **11** 562–73
[60] Coleman J P 1979 *The Electrochemistry of Carboxylic Acids and Derivates: Cathodic Reductions. In Supplement B the Chemistry of Acids Derivatives Part 2* ed S Patai (New York: John Wiley & Sons, Ltd) pp 781–821
[61] Luca O R and Fenwick A Q 2015 Organic reactions for the electrochemical and photochemical production of chemical fuels from CO_2—the reduction chemistry of carboxylic acids and derivatives as bent CO_2 surrogates *J. Photochem. Photobiol.* B **152** 26–42
[62] Nguyen C C and Lucht B L 2018 Development of electrolytes for Si-graphite composite electrodes *J. Electrochem. Soc.* **165** A2154–61